Dorh, N., Stokes, J., & Cryan, M. J. (2015). Polarization and mutual coupling effects in aluminum nanoantenna arrays. Journal of the Optical Society of America B, 32(4), 721-729. DOI: 10.1364/JOSAB.32.000721

Polarisation and Mutual Coupling Effects in Aluminium Nanoantenna Arrays

N. Dorh, J. Stokes and M. J. Cryan

Department of Electrical and Electronic Engineering, University of Bristol, Bristol BS8 1UB, UK
Corresponding author : m.cryan @bristol.ac.uk

Abstract: This paper uses Finite Difference Time Domain (FDTD) modelling to study impact of varying the polarisation of the point source(s) on both the single aluminium dipole nanoantenna and a 2 x 2 array. Starting with the single dipole nanoantenna, this paper demonstrates the strong dependence of the Power Enhancement and resonance on the polarisation of the source by alternating between orthogonal polarisation states. With each element of the array excited by a single point source, the resonance, Power Enhancement and far field radiation patterns are observed as the polarisation of each source is rotated, in varying combinations. The results demonstrate that a unique far field radiation pattern is produced for each polarisation combination, which may lead to applications in sub-diffraction limit imaging and quantum optics.

1. Introduction

The antenna concept has existed for well over a century[1-3] and nanoantennas have now extended the technology into the optics regime; combining classical antenna theory with plasmonics to dramatically enhance the emission and absorption of light [4]. Nanoantennas are nanoscale devices which couple freely propagating light to localised surface plasmons and vice-versa. Applications of the technology range from imaging to photonic circuits and sensors [5-9]. When an optical emitter such as a quantum dot or fluorophore is brought into close proximity to a nanoantenna, Purcell enhanced emission can occur [4, 10, 11]. Alongside this, the nanoantenna shape will produce a particular pattern in the far field, termed the radiation pattern in classical antenna theory. If the antenna is part of a larger periodic array, the array element spacing can give rise to both radiation pattern shaping effects and surface wave propagation on the array; both of which have been widely studied in the RF literature[12] and the latter is termed Surface Lattice Resonances in the optics field[6, 13]. An important and well-known effect in RF antenna arrays is that of mutual coupling. This is where interaction between neighbouring elements in the array modifies the characteristics of the individual antennas. The simplest manifestation of this is detuning of the antenna resonance, thus one cannot simply use the design of a single element to evaluate the resonance of an array. Mutual coupling will also depend strongly on the orientation of emitter near each antenna. This paper will explore these effects through Finite Difference Time Domain (FDTD) modelling [14] and will show how the array far field pattern and resonant wavelength can be used to determine the orientation of emitters [15, 16] with respect to the nanoantenna arrays elements; this could find applications in single molecule fluorescence and quantum optics.

The FDTD modelling is based on single elements and 2 x 2 arrays operating in the blue part of the spectrum, where they will find applications for enhancing fluorescence from many different types of naturally occurring compounds and molecules[17]. Literature[18, 19] has identified several promising materials for use in the near UV region; Al, Ni and Cu, amongst others. Based on a comparison of dielectric properties within the Drude-Lorentz model, Al losses are among the lowest over the 350-440 nm spectral region, making it a sound choice for nanoantenna design. Aluminium based plasmonics also carries a number of benefits: it is considerably cheaper than gold, self-passivates with a roughly 2-3 nm aluminium oxide layer[20] and has relatively low absorbance over a large spectral range [21, 22]

In this paper Section 2 studies a single isolated antenna, considering the mechanism for enhancement and establishing the polarisation dependence. Section 3 shows results for 2 x 2 arrays under varying excitation conditions, with a particular focus on the enhancement and resonance. Section 4 presents and discusses the effects of mutual coupling on the radiation pattern with respect to source polarisation. Far field projections are based solely on fields above the substrate layer (emission into air). Section 5 presents the conclusions.

2. The Single Nanoantenna

Figure 1 shows the basic building block of the work which is a dipole nanoantenna consisting of two 190 nm x 40 nm x 50 nm (l x w x d) aluminium arms separated by a 30 nm gap, in which the electric dipole source is centred. This dipole nanoantenna sits on a 500 nm thick glass substrate (n=1.5) which extends into the lower Perfectly Matched Layer, eliminating any reflection from boundaries of the glass. The aluminium properties are modelled using material constants from the literature[23].

Figure 1: Single aluminium dipole nanoantenna with dipole source *l*=190 nm, *w*=40 nm, *g*=30 nm, *d*=50 nm, *s*= 500 nm, refractive index of glass, *n*=1.5. 350-550 nm Electric dipole source centred in the gap in both the x-y and y-z planes, 25 nm above the substrate surface.

Previous studies [24] demonstrated that a metal nanoantenna structure causes an increase in the radiative decay rate which translates to shorter fluorescence lifetimes and an increase in observed intensity of the light radiated by the source. The wavelength at which this occurs is dependent on both the arm length (l) and the aspect ratio ($^{l}/_{w}$)[10]. The gap length, g, determines the strength of the coupling between the two nanoantenna arms [25] and the light intensity, as observed above the gap, is known to show an inverse cubic dependence on g [7, 24]. In [20], it was demonstrated that Al nanoparticles are stable (in terms of resonance/performance) over time as the initial passivation layer of Al_2O_3 prevents further oxidation and/or deterioration of performance. For this reason, the oxide layer was not included in the simulations presented.

The single aluminium dipole nanoantenna shown in Figure 1 is designed to resonate at 420 nm. In the FDTD simulations, it is excited by a 350-550 nm electric dipole source; first polarised along, then orthogonal, to the long axis of the nanoantenna. The entire structure is bound by Perfectly Matched Layers (PMLs) in all directions. 1 nm uniformed meshing is used over the dipole nanoantenna which gives a satisfactory balance between converge and computational requirements. Purcell's work with single emitters showed the dependence of the emission rate on the local environment[26]. When coupled with a resonant cavity, like a nanoantenna, the enhancement in emission rate is known as the Purcell Factor[26, 27]. In this paper, the Purcell Factor is calculated by normalising the power radiated by the dipole source with the nanoantenna structure in place, to the power that would have been radiated by the source in a homogenous (free-space) medium. Novotny *et al* [28] demonstrated that emission rate is proportional to the local density of states (LDOS) which itself is proportional to power emitted by the source; making this approach to calculating the Purcell Factor (or Enhancement) less computationally intense and equivalent to the more widely known theoretical expression.

Although the Purcell Factor is commonly quoted as a figure-of-merit for fluorescence and single emitter studies, recent literature [29, 30] suggests that, in its original form or isolation, it may not be representative of the efficacy of the nanoantenna system. For example, Barthes *et al* [29] found that the Purcell Factor for an emitter placed near a plasmonic guide (nanowire) was constant despite increasing absorption in the waveguide. This is because the Purcell Factor describes the enhancement in emission from the dipole (source), but does not incorporate the various channels that it may take thereafter, and must therefore be considered with care. This is similar to the case of the Scattering parameters (*S* parameters) used in classic antenna characterisation. In electrical engineering, complex systems can be represented by N-port networks [31], where a port is a point or terminal in the system where power can be applied or received [31]. The input-output relationships between the ports are defined using *S*-parameters of the form S_{pq} where p and q are port numbers [31, 32]. In a two-port network, S_{21}, represents the power received at port 2 from port 1, S_{11} and S_{22} represent the power reflected at ports 1 and 2 respectively. In practice, a low S_{11} would be desirable for an antenna and indicates very little power reflected at the input. However, S_{11} measurements do not discriminate between Ohmic losses and the desired radiation losses; hence, are rarely considered in isolation. In contrast, S_{21}, describes the power transferred from the transmitting to receiving antenna and is a better indicator of how well the device radiates. In this paper, the figure-of-merit is Power Enhancement, defined as the net power transmission through a 3D box enclosing the nanoantenna, normalised to the power that would have been injected by the source in a homogenous free space environment. This approach is analogous to the S_{21} measurement, which, together with the Purcell Factor, can give a more useful representation of the emitter-nanoantenna system.

Figure 2 shows Power and Purcell Enhancement *vs* wavelength for two orthogonal source polarisations. When driven by the E_x polarised source, both the Purcell Factor and Power Enhancement followed a resonant profile with a peak at 420 nm, and maxima of 26 and 18.8 respectively. The relative drop from the Purcell Factor to Power Enhancement seen in Figure 2 is due to light from the source coupling to lossy channels in the nanoantenna, further emphasising the need to consider both figures of merit

when evaluating nanoantenna performance. In contrast, there was no resonance when the single dipole was driven by an E_y polarised source, this shows that the E_y polarised light could not couple to the plasmonic mode of the nanoantenna.

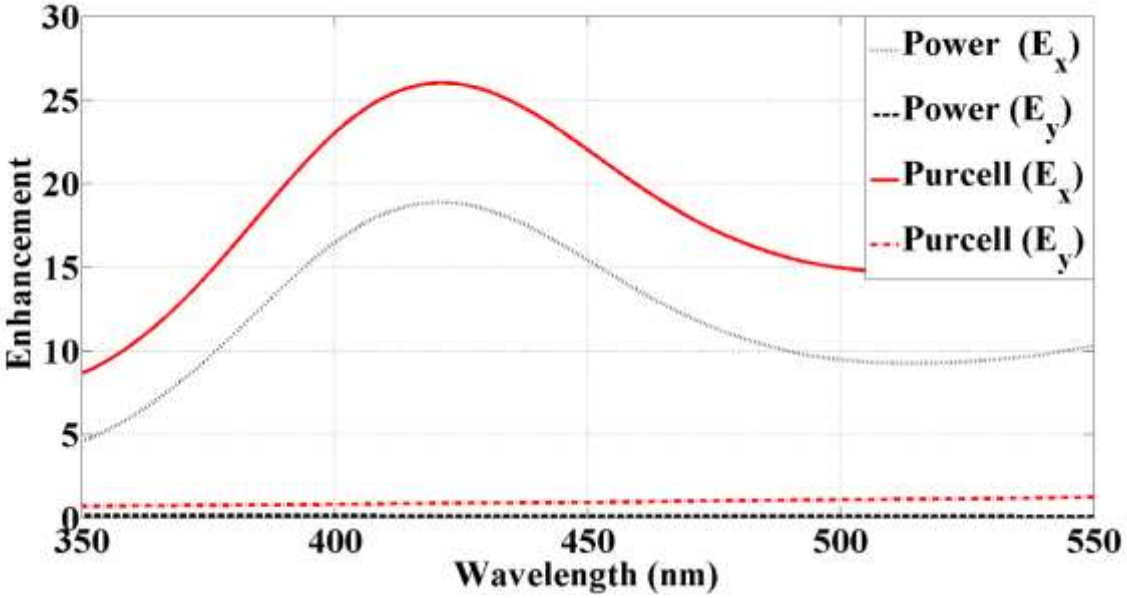

Figure 2: Power and Purcell Enhancement for a single 190 x 40 nm dipole nanoantenna with a 30 nm gap when excited by an E_x and E_y polarised electric dipole source

In Figure 3, we present the spatial distribution of the electric field magnitude as seen at the nanoantenna surface, at resonance, in the *x-y* and *x-z* planes. A 500 nm x 100 nm (*x, y*) planar monitor collects the time domain Electric field data at the nanoantenna surface which is then Fourier transformed to yield the frequency domain plots. Several maxima can be seen along the nanoantenna long axis which is expected for higher order resonance [11]. In the horizontal (*x-y*) plane, the field is symmetric about the centre of gap but asymmetric in the vertical (*x-z*) plane. The strongest field magnitude is observed at the centre of the gap and follows a damped oscillatory profile along each nanoantenna arm. On the nanoantenna arms, the electric field is strongest at the interface between the metal nanoantenna and the dielectric media (air and glass) and decays more quickly in the metal than the dielectric. It is also evident that the field is greater in the glass substrate than the air, due to the relatively higher refractive index of the glass substrate. Light from the E_x polarised source couples into the higher order surface plasmon mode and as these surface plasmons reflect at the nanoantenna boundary, they form localised plasmonic standing waves visible in Figure 3.

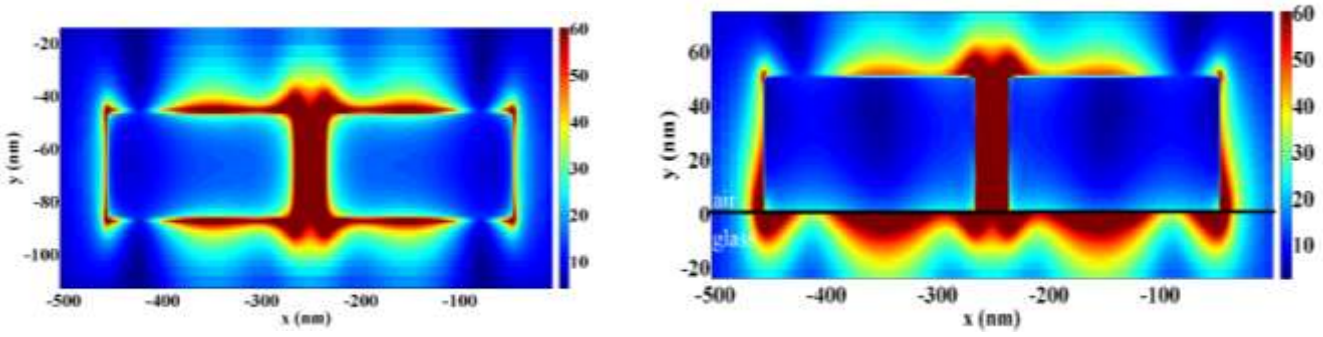

(a) **(b)**

Figure 3: |E| Field distributions at 420 nm as seen from (a) the *x-y* plane at the nanoantenna surface and (b) the *x-z* plane when driven by an E_x polarised dipole source

Figure 4 shows the electric field distribution for the case of an E_y dipole source. Unlike the previous case, the electric field remains concentrated in the gap and plasmonic coupling to the nanoantenna is not evident. The orthogonal polarisation of the source inhibits any coupling to the desired plasmon mode of the nanoantenna.

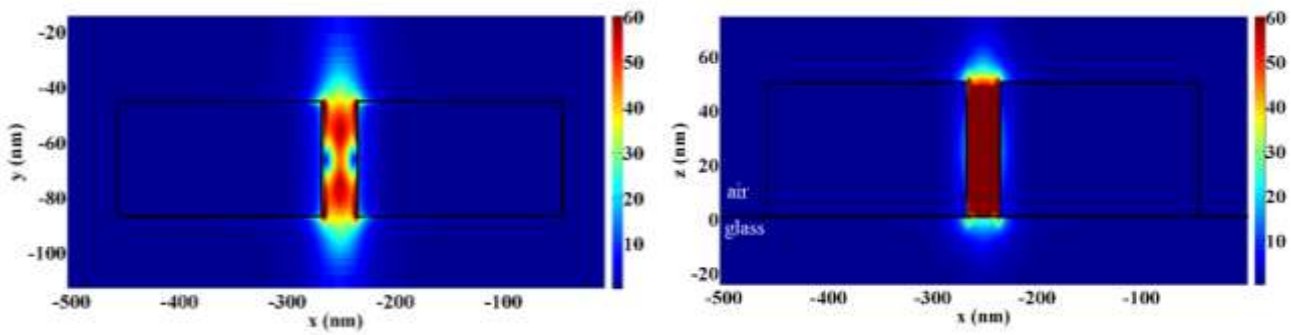

(a) **(b)**

Figure 4:|E| Field distributions at 420 nm wavelength, as seen from (a) the x-y plane at the nanoantenna surface and (b) the x-z plane when driven by an E_y polarised dipole source.

3. Polarisation Dependence of Nanoantenna Planar Arrays

Nanoantennas are now being used and studied in arrays [6, 33-35]. Although arrays add complication to both the design and fabrication, they hold the promise of beam shaping, beam steering and increased sensing volumes. In tests and applications similar to that presented by Stokes *et al* [33], when using emitter-doped polymer layers as the local driving sources, it may not be possible to control the final polarisation of the emitting molecule. Likewise, for fluorescence detection from single molecules, it is imperative to characterise the effects of changing polarisations on the observed enhancement and far field.

In this section, we present a 2 x 2 aluminium dipole nanoantenna array as shown in Figure 5 and explore the effects of different emitter orientations. Each element is separately excited in the gap by identical, coherent dipole sources and polarised either parallel (E_x) or orthogonal (E_y) to the nanoantenna long axis in various combinations, shown in Table 1.

Combination number	**Polarisation**			
	Dipole 1	Dipole 2	Dipole 3	Dipole 4
1	E_x	E_x	E_x	E_x
2	E_y	E_x	E_x	E_x
3	E_y	E_y	E_x	E_x
4	E_y	E_x	E_y	E_x
5	E_y	E_x	E_x	E_y
6	E_y	E_y	E_y	E_x
7	E_y	E_y	E_y	E_y

Table 1: Source excitation combinations. The polarisation of each source was varied such that resulting combinations from 1-7 vary from all sources x-polarised (1) to all sources y-polarised (7).

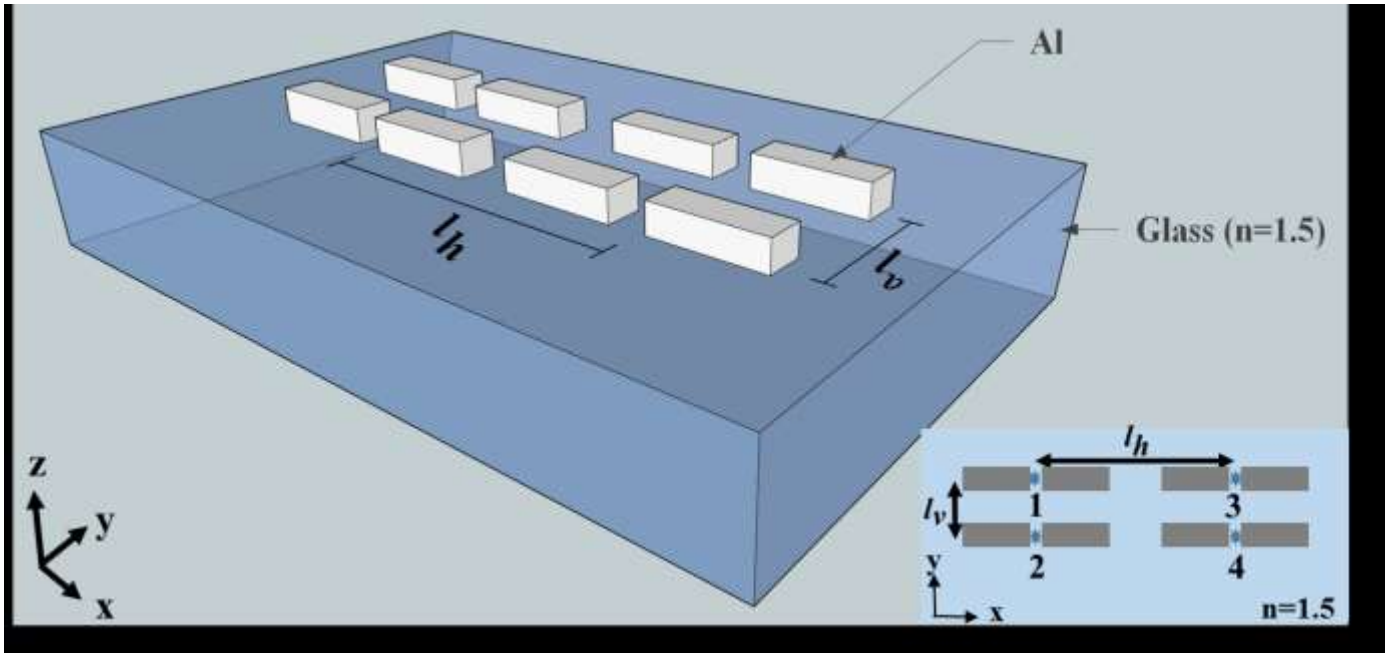

Figure 5: Uniform 2 x 2 array of aluminium nanoantennas with horizontal pitch, l_h=510 nm, and vertical pitch, l_v=140 nm. Each individual dipole nanoantenna based on the dimensions presented in Figure 2 and excited by a single source, numbered 1-4.

In Figure 6, we plot the peak Power Enhancement (at resonance) against the number of *x*-polarised sources for combinations 1-7 of Table 1. The maximum Power Enhancement of 15.9 is achieved when all four sources are E_x polarised (combination 1) and minimum of 4.5 when all but one source is E_y polarised (combination 6). Source polarisation affects the ability of incident radiation to couple to the plasmonic mode of the nanoantenna. As previously discussed, only the E_x sources couple to the plasmon mode of the nanoantenna structure and subsequently yield enhancement. In general, Power Enhancement increases almost linearly with each additional E_x polarised source (combinations 2-6). Combinations 2-4, all contain only 2 E_x sources, however, they are placed horizontally, vertically and diagonally, with respect to each other. Figure 6 shows that under those conditions, there is a noticeable fluctuation in the peak enhancement. It can be inferred that, the enhancement not only depends on the number of excited nanoantennas in the array but also the relative locations of these nanoantennas with respect to each other within the array. This effect also appears in classical antenna arrays, and is often exploited to engineer beam properties such as shape and direction.

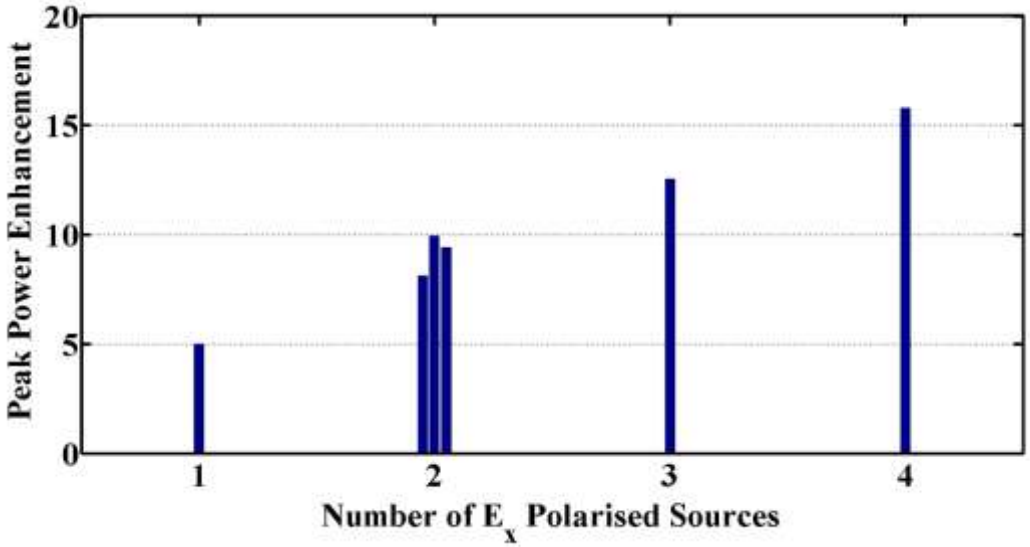

Figure 6: Bar chart of Power Enhancement *vs* Number of *x*-polarised sources. Combination 1 in Table 1 has 4 E_x polarised sources and shows the maximum enhancement.

In Figure 7, we plot the resonant wavelength against the excitation combinations used. For ease of comparison, we include combination number 1/1 which relates to the case of a single E_x driven antenna within the 2 x 2 array. Prior to any changes in the

polarisation of the sources, two resonance shifts can be seen when the dipole nanoantenna is placed in the 2 x 2 array. Firstly, the presence of the other nanoantennas (numbers 2-4, see Figure 5) within the array, induces a red shift of the single nanoantenna 1's resonance to 426 nm from 420nm for a single isolated antenna (see Figure 2). Secondly, when nanoantennas 2-4 were driven with identical E_x polarised sources; there is a blue shift of roughly 16 nm. For source combinations 1-6, the number of E_x polarised sources gradually reduces from 4 to 1, resulting in a linear red shift of the resonance back to 426 nm.

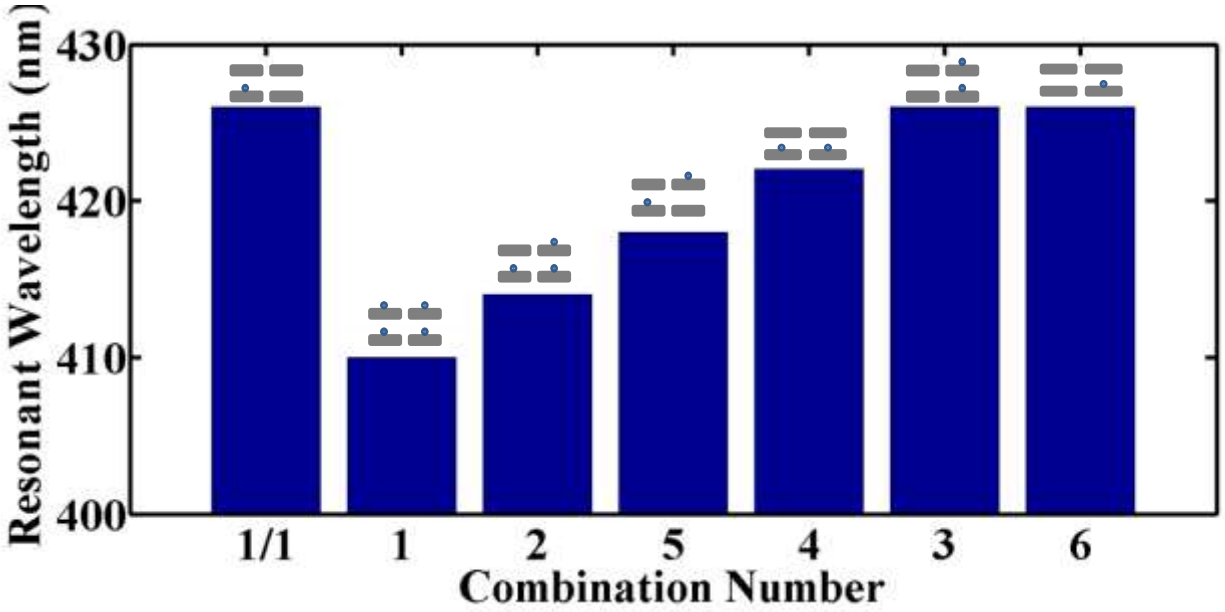

Figure 7: Bar chart showing resonant wavelength variation with source combinations as shown in Table 1. 1/1 is the case of a single driven antenna within the 2 x 2 array and resonates at 426 nm which is 6 nm red shifted with respect to the single isolated nanoantenna (420nm). On the inset, each bar represents a dipole nanoantenna and the dot relates to an E_x polarised source the remaining sources are E_y polarised (not shown); in the 1/1 case the dot represents the only source present in the simulation.

Considering the earlier classical antenna comparison, it is common that when antennas are placed in arrays, some of the energy destined for the far field, may interact with other elements in the array. This is known as mutual coupling and is dependent on the relative orientations and spacing between antenna elements [36]. Consider the 2 x 2 array shown in Figure 5, it is expected that most of the light leaving nanoantenna 1 will radiate into the far field, however, a substantial proportion will be directed at nanoantennas 2-4. Some of this light will re-couple into plasmons before being scattered again to the far field or other nanoantennas, while some will interfere with the dipole sources directly (mutual impedance) or couple to lossy channels. Mutual coupling is a complex process with noticeable effects on the behaviour of the array. In general, coupling effects are directly proportional to the number of E_x polarised sources, as can be seen in Figure 6 and 7.

Figure 8 shows the Power Enhancement spectra for combinations 3-5; although in all three cases, only 2 E_x polarised sources were present, the spectra can be easily distinguished. When the two E_x polarised sources are oriented diagonally (combination 5), the resulting Power Enhancement spectrum is narrowest and broadens for both horizontal (combination 4) and vertical (combination 3) orientations. The highest Power Enhancement is achieved when the two sources are diagonally positioned within the array and lowest when arranged vertically. In terms of resonant wavelength, the diagonal case has the largest detuning from the single excited nanoantenna case and the amount of detuning can be taken as a measure of the strength of the coupling between the nanoantennas. These interactions are mainly governed by the radiation pattern of the individual antennas and since we are operating in a higher order resonance, they are not those expected for conventional fundamental mode RF dipole antennas. In section 4, we will calculate the higher order mode radiation patterns and will discuss Figure 8 with reference to these patterns.

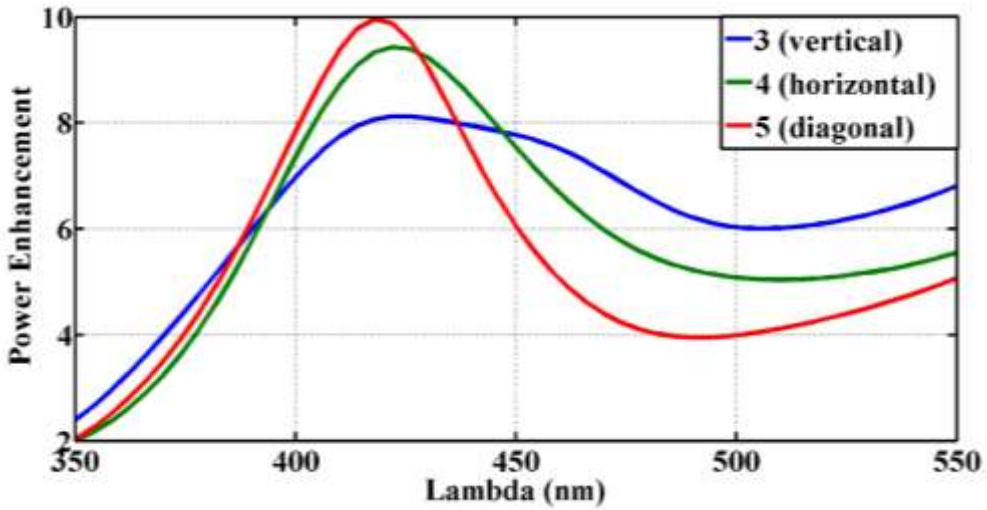

Figure 8: Power Enhancement vs wavelength for source combinations 3-5

In Figure 9, we plot the electric field intensity maps at the array surface, for combinations 3-5, to establish the underlying changes which influence the array characteristics. These maps show the interaction of fields among the array elements and allow us to make some useful qualitative observations. As previously mentioned, elements in the array may couple in several ways which will affect array performance differently. Combining the information presented in Figure 8 and 9 gives further insight into the type of coupling occurring in each case.

In Figure 9a, the two E_x sources are positioned vertically with respect to each other; strongest field intensities are observed around the E_x driven nanoantennas. Small, identical 'hot spots' can be seen at the outer edges of all the nanoantenna arms, suggesting little scattering from these sharp corners. Field lines between the two E_x driven elements are mostly confined to the line connecting the two sources, and the mode shape on the faces of the dipole nanoantennas arms opposite to other arms, appears more damped than those facing free space.

In Figure 9b, with the E_x driven elements horizontally oriented with respect to each other (combination 4), there are more field lines extending towards the other elements in the array. The mode shape now more closely resemble that seen in Figure 2 and more 'hot spots' are visible on both the E_x and E_y driven elements; appearing stronger between adjacent nanoantennas.

In Figure 9c, we observe that the strongest field intensities on the E_y driven elements occur in combination 5; the field distributions at the gaps are almost identical and 'hot spots' are present with greater intensity at all nanoantenna boundaries. Earlier it was established that the electric field remains strongly confined to the gap when the nanoantenna is driven by an E_y source. We can therefore conclude that any scattering or 'hot spots' would be as a direct result of fields induced by the E_x sources within the array. Figure 9 shows qualitatively that there is increasing coupling from 9a to 9c; this links to Figure 8 where detuning increases from combination 3 to combination 5.

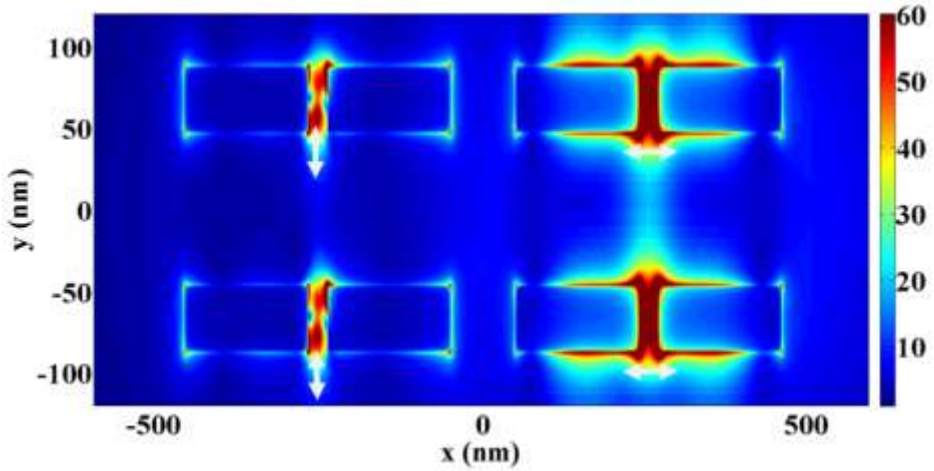

(a)

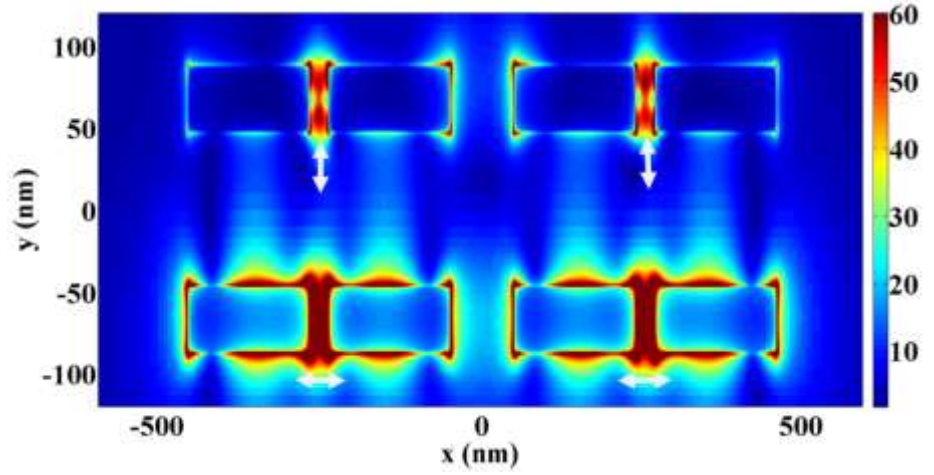

(b)

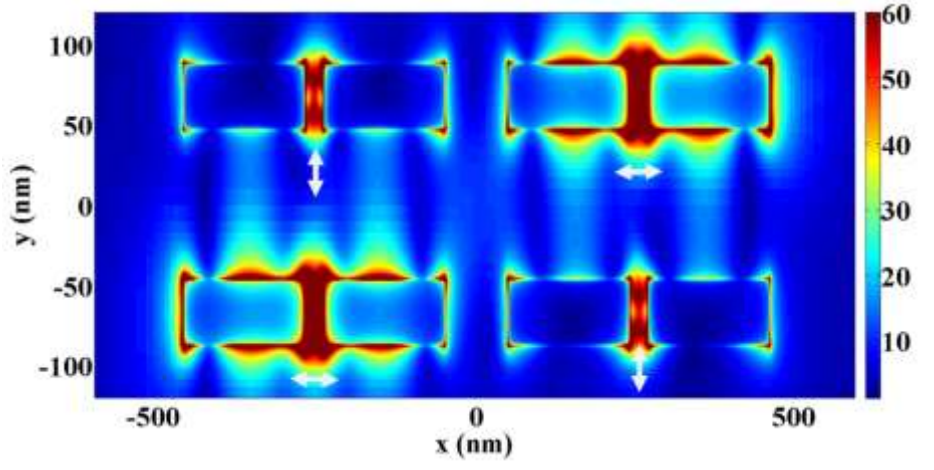

(c)

Figure 9: |E| Field distribution at array surface under illumination from source combinations 3-5 in Table 1; two of the dipole sources were E_x polarised and the other two were E_y polarised, such that the two E_x sources were aligned (a) vertically/combination 3 λ=426 nm (b) horizontally/combination 4 λ=422 nm and (c) diagonally/combination 5 with respect to each other, λ=418 nm

4. Polarisation, Mutual Coupling and the Far Field

In this section, we will consider the effects of varying the polarisation of the sources, on the radiation pattern of the nanoantenna array. The far field radiation pattern is the vector sum of the response of individual nanoantennas and the complex interactions between the array elements [12]. The glass substrate introduces anisotropy to the surrounding medium which can pose a challenge for conventional far field projections. One common solution uses the fields emitted in the air to calculate the far field above the

structure. Figure 10a shows a transverse section, parallel to the long axis, through the far field radiation pattern produced by FDTD modelling of a single isolated 190 x 40 nm aluminium dipole nanoantenna (see Figure 2) for varying mesh sizes. It shows that the results converge for mesh sizes below 2 nm, validating our choice of 1 nm meshing. The beam shape is directly related to the multi-polar resonance formed along the nanoantenna surface and is typical of the second eigenmode of the nanoantenna geometry [11]. There are two main emission peaks near ±45° each with beamwidths (Full Width Half Maximum (FWHM)) of 43° and a small single side lobe at 0°.

In Figure 10b, we show a transverse section through the far field radiation patterns of both the single nanoantenna and a 2 x 2 array of the same dipole nanoantennas in the ideal excitation scenario; all sources E_x polarised and coherent. For ease of comparison, the field intensities are normalised to the respective maxima and plotted on a common vertical dB axis. Compared to the single nanoantenna, the general beamshape remained unchanged except for narrowing of the beamwidth to 28° and two additional side lobes at ±20°. The narrowing and side lobe formation are as a result of the additional elements in the same emission plane and is common in antenna arrays. Also noteworthy, the emission peaks of the array have shifted by 7° to ±52° and resonant wavelength blue shifts by 10 nm to 410 nm in the case of the array.

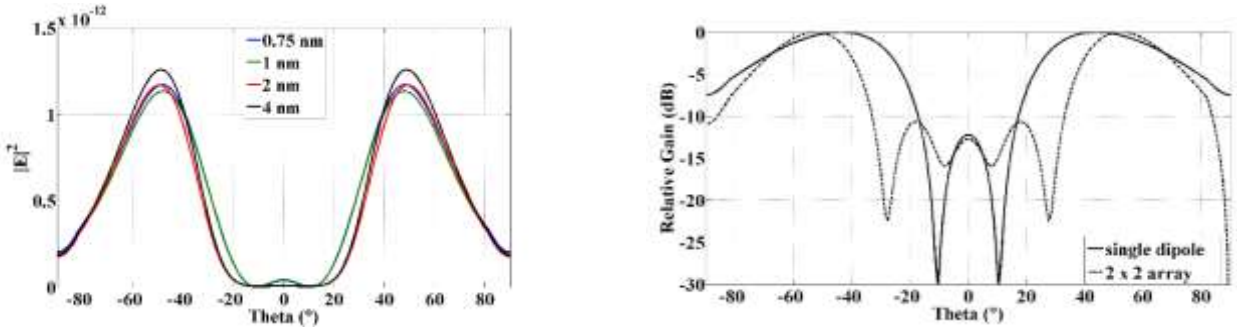

(a) (b)

Figure 10: (a) Far field radiation pattern for a single isolated dipole nanoantenna at resonance, 420 nm for varying mesh sizes; results converge for mesh sizes below 2 nm(b) Transverse section through the far field projections of the single dipole nanoantenna and a 2 x 2 array of identical dipole nanoantennas all excited by E_x sources and at resonance, 410 nm. For ease of comparison, field intensities are normalised to their respective maxima and plotted on a common dB axis. (Where Theta=0º is emission along the positive *z*-axis in Figure 5)

Scatterers, such as nanoantennas, when placed in an array, will tend to interact electromagnetically; this is well known in the classical antenna world as mutual coupling [36] and in the nanoantenna world as dipole interaction [6]. In the absence of mutual coupling within an array, any currents or field distributions on a given array element are independent of the other elements within that array. Provided the structures and excitation conditions are identical, the overall far field response can readily be determined using a classical antenna concept called Pattern Multiplication [12].

Pattern multiplication states that for a uniform array of *N* identical antennas, the radiation pattern of the array is given by the product of the Array Factor (AF) and the radiation pattern of a single element *U*. The emission characteristics of an array of antennas are described by the AF. The AF is a complex vector function of element spacing, *d*, amplitude weighting, *a*, relative phase weightings, β, the incident electromagnetic (EM) wave with wave vector *k* and phase θ and number of antenna elements, *N*. The resulting expression for the far field radiation pattern of the array, U_{array}, is:

$$U_{array} = U\sum_{n=1}^{N} a_n e^{j(n-1)(kd\cos(\theta)+\beta)} \quad (1)$$

Pattern Multiplication neglects any coupling between array elements and therefore allows us to investigate the effects of mutual coupling. By applying appropriate substitutions into (1) we can therefore investigate the impact of mutual coupling on the resulting far field radiation patterns when the polarisation of the sources are varied in different combinations.

As previously discussed, the sources are all coherent, therefore we can apply zero phase weighting and initial phase of zero. The element spacing is normalised to the resonant wavelength of the single nanoantenna. In Figure 11, we plot the far field patterns of the 2 x 2 array excited by combinations 3 and 5 with and without the E_y sources present. It shows that the presence of the E_y sources does not significantly affect the far field pattern. As a result, for simplicity, we apply binary amplitude weighting of 0 to E_y driven elements, and 1 to E_x driven elements. Finally, the single nanoantenna radiation pattern from FDTD can then be substituted into (1), with varying amplitude weightings, corresponding to the different excitation combinations, to produce the Pattern Multiplication approximation of the far field response.

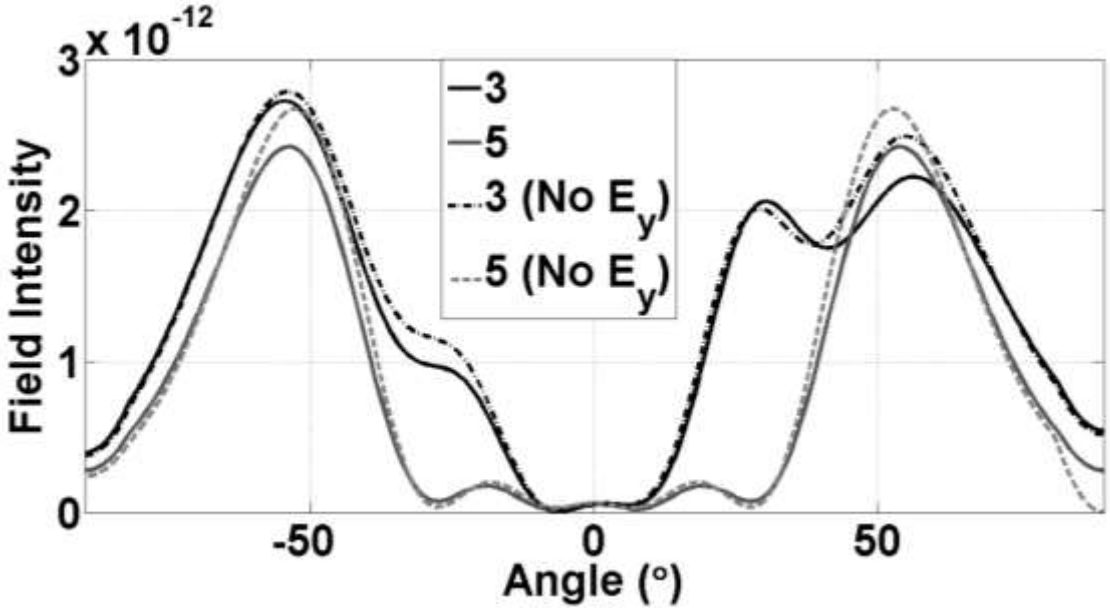

Figure 11: Far field radiation patterns of 2 x 2 aluminium nanoantenna array excited using combinations 3 and 5 with and without the Ey sources included in the FDTD simulation.

In Figure 12, we plot a transverse section parallel to the long axis, through the radiation patterns produced by Pattern Multiplication and FDTD when the 2 x 2 nanoantenna array is excited using combination 3. The Pattern Multiplication plot is symmetric about 0° with the main emission peaks at ±50°, 3 side lobes centred at 0° and ± 20°, as well as 4 nulls at ±11° and ±24°. The FDTD plot, however, is asymmetric about 0°, the main emission peaks lie at ±55°and there is a single null at -6°. From these plots, it can be inferred that, due to mutual coupling, the side lobes near ± 20° possibly merged with the main lobes; cancelling 3 of the 4 nulls and generating secondary peaks on the main lobes.

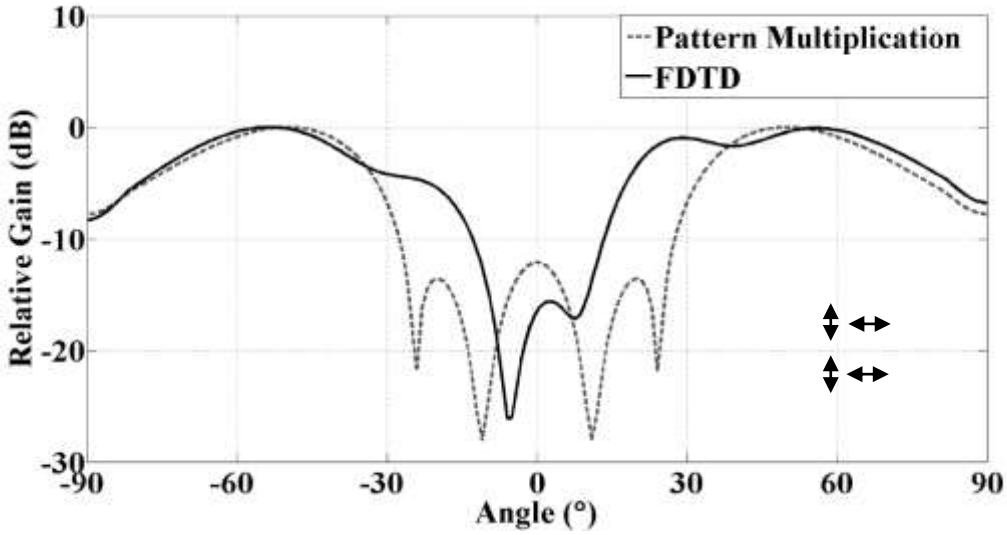

Figure 12: Transverse section through the long axis, of the radiation pattern of a 2 x 2 aluminium dipole nanoantenna array produced using Pattern Multiplication and FDTD with excitation combination 3.

The phase and amplitudes of the electric field along the nanoantenna surfaces contribute to the far field properties and due to mutual coupling become interdependent. The self-impedances, of nanoantennas in isolation, are replaced with the concept of active impedance [37], which is the combination of the self-impedance and mutual impedance. Mutual impedance describes the relationship between the current on the driven antenna and the voltage induced on another antenna in the array [38, 39]. By definition, it is expected that the mutual impedance will vary with polarisation of the sources and would therefore yield uniquely identifiable far field patterns.

In Figure 13, we observe the far field radiation patterns calculated by FDTD for the 2 x 2 array under excitation conditions 1, 3 and 5. Under combination 1, the radiation pattern is symmetric about the 0° and 90° lines with emission peaks at ±52°. Combinations 3 and 5 relate to two E_x and two E_y sources arranged vertically and diagonally, respectively and there is a clear distinction between the two far field patterns. The far field pattern from combination 3 is asymmetric about the 90° azimuthal angle whereas the pattern from combination 5 is symmetric. In addition, we observe an additional side lobe at elevation angle of 20° with combination 3 and the pattern from combination 5 is rotated with respect to combination 3. This is due to the diagonal symmetry of the near field distribution across the array seen in Figure 9.

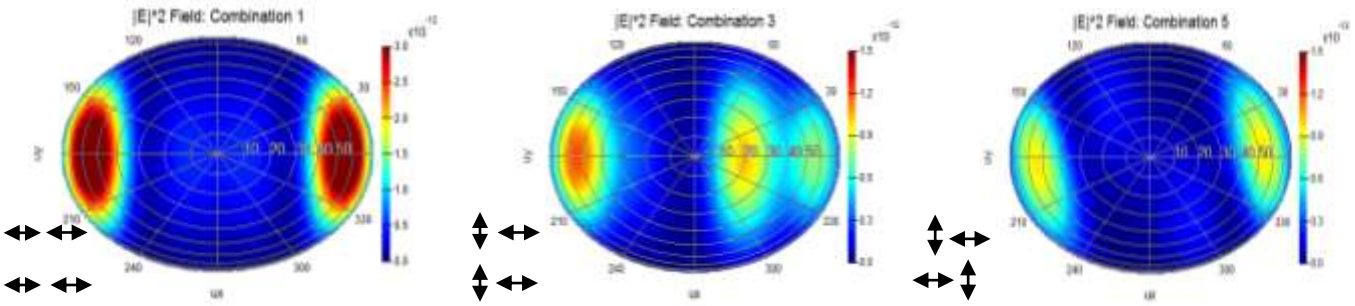

Figure 13: FDTD far field radiation patterns for the 2 x 2 aluminium dipole nanoantenna array excited using combination (a) 1 (b) 3 and (c) 5; arrows indicate the polarisation of each source

Figure 14 shows the transverse section through the long axis, of the radiation patterns for the 2 x 2 nanoantenna array excited using combinations 1, 3, 5 and 6. The vertical scale was kept as field intensity ($|E|^2$), to highlight some key features. Firstly, it is evident that the field intensity varies significantly with the polarisation of the sources, as discussed earlier. From the graph, it is clear that the beam shape also depends on the source polarisations. Excitation using combination 3, for example, results in a far field radiation pattern that is asymmetric about 0° whereas the pattern from combination 5 is symmetric. In addition, we observe secondary peaks on the main lobes with combination 3 but well defined side lobes near ±20° from combination 5. There are also some similarities between the shape of the far field radiation patterns for combinations 1 and 5, and likewise combinations 3 and 6. However, it holds that for the radiation patterns that are similar in shape, the peak field intensities are significantly different.

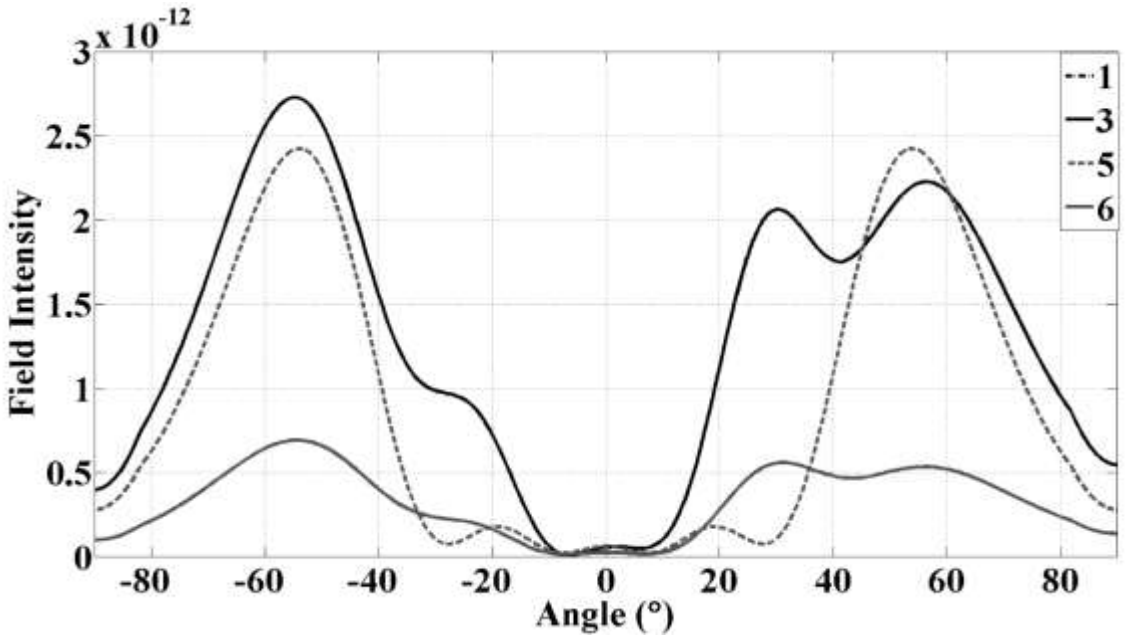

Figure 14: FDTD calculated far field projections for the 2 x 2 aluminium nanoantenna array using source combination 1, 3, 5 and 6.

The radiation patterns in Figures 10, 11 and 12 show that unlike the fundamental mode in a dipole antenna which has an almost omnidirectional radiation pattern [12] with a maximum normal to the antenna axis, this higher mode has a minimum. This results in the coupling and detuning effects seen above where diagonally oriented (combination 5) sources give much more detuning than vertically aligned ones (combination 3). This highlights the flexibility that antenna array can give through choices of individual antenna modes, array spacing and array size.

5. Conclusions

This paper explores the potential for harnessing the effects of polarisation and mutual coupling within a nanoantenna array for identifying the characteristics of the excitation sources. Power Enhancement, in contrast to Purcell Enhancement, is used to quantify the amount of emission enhancement for the nanoantenna-emitter system. Starting with a single aluminium dipole nanoantenna, by switching between orthogonal polarisations, it becomes evident that the Power Enhancement depends strongly on the polarisation of the source. When placed within a 2 x 2 array of nanoantennas, the dependence on polarisation of individual sources strongly influences the interactions between the nanoantenna elements. As the source polarisation is switched between orthogonal states in varying combinations, both the resonant wavelength and Power Enhancement show a linear relationship with the number of sources polarised along the nanoantenna long axis. In the near field region, the polarisation dictates the mode of interaction (mutual coupling) between elements within the array, resulting in noticeable changes in far field properties. These results suggest that the source orientations become identifiable from the far field radiation patterns. Mutual coupling cannot be avoided in antenna arrays and has traditionally been considered an adverse effect, however, we have demonstrated that it can be harnessed to provide useful information about the sources. These results may lead to applications in sub-diffraction limit imaging and quantum optics.

Acknowledgement : The Authors acknowledge funding from ABB Corporate Research

References

[1]. H. Hertz, "Uber electrodynamische Wellen im Luftraume und deren Reflexion," Annalen der Physik und Chemie **270**, 609-623 (1888).

[2]. H. Hertz, *Electric waves: being researches on the propagation of electric action with finite velocity through space* (Dover Publications, 1893).

[3]. J. D. Kraus, "Antennas since Hertz and Marconi," Antennas and Propagation, IEEE Transactions on **33**, 131-137 (1985).

[4]. P. Bharadwaj, B. Deutsch, and L. Novotny, "Optical Antennas," Advances in Optics and Photonics **1**, 46 (2009).

[5]. N. Liu, M. L. Tang, M. Hentschel, H. Giessen, and A. P. Alivisatos, "Nanoantenna-enhanced gas sensing in a single tailored nanofocus," Nat Mater **10**, 631-636 (2011).

[6]. B. Ng, S. M. Hanham, V. Giannini, Z. C. Chen, M. Tang, Y. F. Liew, N. Klein, M. H. Hong, and S. A. Maier, "Lattice resonances in antenna arrays for liquid sensing in the terahertz regime," Optics Express **19**, 14653-14661 (2011).

[7]. J. L. Stokes, Y. Yu, Z. H. Yuan, J. R. Pugh, M. Lopez-Garcia, N. Ahmad, and M. J. Cryan, "Analysis and design of a cross dipole nanoantenna for fluorescence-sensing applications," J. Opt. Soc. Am. B **31**, 302-310 (2014).

[8]. R. Ahijado-Guzmán, J. Prasad, C. Rosman, A. Henkel, L. Tome, D. Schneider, G. Rivas, and C. Sönnichsen, "Plasmonic Nanosensors for Simultaneous Quantification of Multiple Protein–Protein Binding Affinities," Nano Letters **14**, 5528-5532 (2014).

[9]. J. C. Reed, H. Zhu, A. Y. Zhu, C. Li, and E. Cubukcu, "Graphene-Enabled Silver Nanoantenna Sensors," Nano Letters **12**, 4090-4094 (2012).

[10]. P. Mühlschlegel, H. J. Eisler, O. J. F. Martin, B. Hecht, and D. W. Pohl, "Resonant Optical Antennas," Science **308**, 1607-1609 (2005).

[11]. T. H. Taminiau, F. D. Stefani, and N. F. van Hulst, "Optical Nanorod Antennas Modeled as Cavities for Dipolar Emitters: Evolution of Sub- and Super-Radiant Modes," Nano Letters **11**, 1020-1024 (2011).

[12]. C. A. Balanis, "Arrays: Linear, Planar, Circular," in *Antenna Theory Analysis and Design Third Edition*(John Wiley and Sons, 2005), pp. 283-296.

[13]. A. I. Väkeväinen, R. J. Moerland, H. T. Rekola, A. P. Eskelinen, J. P. Martikainen, D. H. Kim, and P. Törmä, "Plasmonic Surface Lattice Resonances at the Strong Coupling Regime," Nano Letters **14**, 1721-1727 (2013).

[14]. "Lumerical FDTD Solutions," (Lumerical Solutions, Inc).

[15]. M. A. Lieb, J. M. Zavislan, and L. Novotny, "Single-molecule orientations determined by direct emission pattern imaging," J. Opt. Soc. Am. B **21**, 1210-1215 (2004).

[16]. A. S. Backer, M. P. Backlund, M. D. Lew, and W. E. Moerner, "Single-molecule orientation measurements with a quadrated pupil," Opt. Lett. **38**, 1521-1523 (2013).

[17]. K. Ray, M. H. Chowdhury, and J. R. Lakowicz, "Aluminum Nanostructured Films as Substrates for Enhanced Fluorescence in the Ultraviolet-Blue Spectral Region," Analytical Chemistry **79**, 6480-6487 (2007).

[18]. K. Aslan, and C. D. Geddes, "Directional Surface Plasmon Coupled Luminescence for Analytical Sensing Applications: Which Metal, What Wavelength, What Observation Angle?," Analytical Chemistry **81**, 10 (2009).
[19]. J. M. McMahon, G. C. Schatz, and S. K. Gray, "Plasmonics in the ultraviolet with the poor metals Al, Ga, In, Sn, Tl, Pb, and Bi," Physical Chemistry Chemical Physics **15**, 5415-5423 (2013).
[20]. J. Martin, J. Proust, D. Gérard, and J. Plain, "Localized surface plasmon resonances in the ultraviolet from large scale nanostructured aluminum films," Optical Materials Express **3**, 954-959 (2013).
[21]. A. Mohammadi, V. Sandoghdar, and M. Agio, "Gold, Copper, Silver and Aluminum Nanoantennas to Enhance Spontaneous Emission," Journal of Computational and Theoretical Nanoscience **6**, 2024-2030 (2009).
[22]. M. W. Knight, L. Liu, Y. Wang, L. Brown, S. Mukherjee, N. S. King, H. O. Everitt, P. Nordlander, and N. J. Halas, "Aluminum Plasmonic Nanoantennas," Nano Letters **12**, 6000-6004 (2012).
[23]. E. D. Palik, *Handbook of Optical Constants of Solids* (Academic Press, 1997).
[24]. O. L. Muskens, V. Giannnini, J. A. Sanchez-Gil, and J. Gomez Rivas, "Strong Enhancement of Radiative Decay Rate of Emitters by Single Plasmonic Nanoantennas," Nano Letters **7**, 5 (2007).
[25]. V. Giannini, A. I. Fernández-Domínguez, S. C. Heck, and S. A. Maier, "Plasmonic Nanoantennas: Fundamentals and Their Use in Controlling the Radiative Properties of Nanoemitters," Chemical Reviews **111**, 3888-3912 (2011).
[26]. E. M. Purcell, "Spontaneous emission probabilities at radio frequencies," (1946), p. 681.
[27]. A. F. Koenderink, "On the use of Purcell factors for plasmon antennas," Opt. Lett. **35**, 4208-4210 (2010).
[28]. L. Novotny, and B. Hecht, "Light emission and optical interactions in nanoscale environments," in *Principles of Nano-Optics*(Cambridge University Press, 2006), pp. 251-300.
[29]. J. Barthes, A. Bouhelier, A. Dereux, and G. C. d. Francs, "Coupling of a dipolar emitter into one-dimensional surface plasmon," Sci. Rep. **3** (2013).
[30]. C. Sauvan, J. P. Hugonin, I. S. Maksymov, and P. Lalanne, "Theory of the Spontaneous Optical Emission of Nanosize Photonic and Plasmon Resonators," Physical Review Letters **110**, 237401 (2013).
[31]. D. M. Pozar, "The Scattering Matrix," in *Microwave Engineering Third Edition*(John Wiley and Sons, 2005), pp. 174-197.
[32]. R. Chatterjee, "Scattering and Impedance Matrix Representation of Microwave Junctions," in *Advanced Microwave Engineering: Special Advanced Topics*(Ellis Horwood Limited, 1988), pp. 111-122.
[33]. J. L. Stokes, P. Bassingdale, J. W. Munns, Y. Yu, G. S. Hilton, J. R. Pugh, A. Yang, A. Collins, P. J. Heard, R. Oulton, A. Sarua, M. Kuball, A. J. Orr-Ewing, and M. J. Cryan, "Direct Measurement of the Radiation Pattern of a Nanoantenna Dipole Array," presented at the European Conference on Integrated Optics ECIO2012, Sitges, Barcelona, Spain, April 2012.
[34]. A. Kabiri, E. Girgis, and F. Capasso, "Buried Nanoantenna Arrays: Versatile Antireflection Coating," Nano Letters **13**, 6040-6047 (2013).
[35]. M. Laroche, S. Albaladejo, R. Carminati, and J. J. Sáenz, "Optical resonances in one-dimensional dielectric nanorod arrays: field-induced fluorescence enhancement," Opt. Lett. **32**, 2762-2764 (2007).
[36]. C. A. Balanis, "Mutual Coupling in Arrays," in *Antenna Theory Analysis and Design Third Edition*(John Wiley and Sons, 2005), p. 478.
[37]. C. Shuguang, and R. Iwata, "Mutual coupling effects in microstrip patch phased array antenna," in *Antennas and Propagation Society International Symposium, 1998. IEEE*(1998), pp. 1028-1031 vol.1022.
[38]. C. A. Balanis, "Mutual Impedance Between Linear Elements," in *Antenna Theory Analysis and Design Third Edition*(John Wiley and Sons, 2005), p. 468.
[39]. J. D. Kraus, and R. J. Marhefka, "Mutual Impedance of Two Parallel Linear Antennas," in *Antennas for All Applications Third Edition*(McGraw-Hill 2002), p. 448.